Research Paper
Computational Methods for Differential Equations
http://cmde.tabrizu.ac.ir
Vol. *, No. *, *, pp. 1-18
DOI:10.22034/cmde.2026.73438.3750

Identifiability before enrichment: A domain-decomposed spectral-collocation study of a delayed, fractional-order glucose–insulin–glucagon minimal model

Cenk Keşan[1,*] **and Filiz Ülkü Keşan**[2]

[1]Department of Mathematics and Science Education, Buca Faculty of Education, Dokuz Eylül University, İzmir, Türkiye.

[2]Department of Nutrition and Dietetics, Faculty of Health Sciences, Nişantaşı University, Istanbul, Türkiye.

Abstract

Fractional-order and delayed extensions of the Bergman minimal model are increasingly enriched with further mechanisms, most recently glucagon regulation, yet the added parameters, including the fractional orders themselves, must be estimated from the same limited intravenous glucose tolerance test data. We formulate a four-state delayed glucose–insulin–glucagon model with component-wise Caputo derivatives in a dimensionally consistent form, and solve it with a domain-decomposed hybrid Chebyshev–Legendre operational-matrix collocation scheme in which the delay breakpoints and threshold-switching instants are subdomain interfaces. On the resulting forward solver we carry out a Fisher-information identifiability analysis based on the singular values of the whitened sensitivity matrix, with the fractional orders treated as unknown parameters. Under glucose and insulin sampling, ten of the eighteen parameters, including the memory order of the unobserved insulin-action compartment, are not practically identifiable; the parameters of the unobserved compartments account for these losses. An additional glucagon assay restores the glucagon block but not the insulin-action block. The results indicate that enrichment of the minimal model can introduce parameters that standard data do not determine.

Keywords. Glucose–insulin–glucagon model, Fractional-order delay differential equations, Caputo derivative, Spectral collocation, Operational matrix, Parameter identifiability, Fisher information.

2010 Mathematics Subject Classification. 65L03, 65M70, 92C50, 34K37, 93B30.

Uncorrected

1. Introduction

The regulation of blood glucose by insulin is one of the most intensively modelled control problems in physiology, both because of the clinical burden of diabetes and because the underlying feedback loop is compact enough to be captured by low-dimensional dynamical systems. Since its introduction, the Bergman minimal model has served as the workhorse of the field: a small nonlinear system relating plasma glucose, a remote insulin-action compartment, and plasma insulin, whose parameters are estimated from the frequently sampled intravenous glucose tolerance test (FSIGT/IVGTT) [9, 10, 30]. A defining feature of the minimal model is that insulin does not act instantaneously: its effect is routed through a remote compartment, so that a physiological latency is built into the model from the outset [9]. Comprehensive reviews document the many variants proposed since and the estimation machinery built around them [31].

Over the last few years the dominant trend has been to enrich the minimal model, and two enrichments recur. The first replaces integer-order derivatives by fractional (typically Caputo) derivatives, motivated by the claim that metabolic tissues exhibit memory and anomalous diffusion that a single-order local operator cannot represent [22, 23]. This has produced a rapidly growing body of numerical studies: fractional Bergman and glucose–insulin systems solved by transform and fixed-point methods [13], by predictor–corrector and discretisation schemes [3, 6], by residual power series and generalized Runge–Kutta methods [2], by successive approximation and fractional Adams–Bashforth–Moulton (ABM) schemes [4], by hybrid Caputo–Lagrange discretisation [5], and by Laplace–Adomian and generalized

Received: 06 July 2026; Accepted: 15 November 2026.
∗ Corresponding author. Email: cenk.kesan@deu.edu.tr.

Euler techniques [29, 34]. Several of these adopt component-wise fractional orders, assigning a distinct memory depth to glucose, insulin action and secretion [4, 5]. The second enrichment reinstates an explicit discrete time delay τ in the pancreatic sensing of glucose, reflecting the finite time between a glucose signal and the secretory response; this converts the model into a delay—and, in the fractional case, a fractional delay—differential system [5, 31]. In the broader numerical literature, high-order schemes for fractional integro-differential equations, including problems with time delay, neutral delay and distributed-order operators, have recently been developed on the basis of finite block, Lagrange-polynomial and spectral discretisations [1, 15, 17–20], and the available methods for the time-fractional diffusion equation have been reviewed in [16]. These works concern accuracy and stability of the discretisation; the question addressed here, namely whether the parameters of such models can be recovered from data, is complementary.

A third enrichment is now actively advocated: the incorporation of glucagon, the principal counter-regulatory hormone. Recent fractional studies close by explicitly recommending that future models add hormonal regulation together with validation against clinical data [34]. This direction is well grounded. Glucagon has long been represented as a single plasma pool with first-order clearance and a pancreatic release term activated when glucose falls, acting on the liver in opposition to insulin [35]; minimal-model-style formulations couple glucose, insulin, glucagon and pancreatic secretion in a four-subsystem structure [7], compartmental models represent the glucose-driven activation of both insulin and glucagon secretion [27], and glucagon kinetics and its insulin-mediated inhibition during a glucose challenge have been quantified [28]. Fractional glucose–insulin–glucagon systems with memory kernels have also appeared [8]. A four-state, delayed, fractional-order glucose–insulin–glucagon minimal model is therefore not an arbitrary construction but the natural convergence point of these three enrichment programmes.

Each enrichment, however, adds parameters—clearance and coupling constants for glucagon, the delay τ, and, crucially, the fractional orders themselves—that must be inferred from the same limited IVGTT data, in which typically only glucose and insulin are sampled at a few dozen time points. Whether these parameters are recoverable from such data is a question of identifiability, and it is not benign even for the classical model: the minimal model was shown two decades ago to possess numerical non-identifiability regions, with the insulin-sensitivity parameter unrecoverable in a substantial fraction of subjects [32]. Subsequent work confirms that glucose-regulation parameters are frequently only practically identifiable under favourable sampling: profile-likelihood analyses report unidentifiable secretion parameters under standard calibration [14], structurally identifiable insulin-kinetic parameters collapse once realistic assay noise is added [12], bihormonal glucose models exhibit practically unidentifiable parameters under profile likelihood [26], and ultradian models are acknowledged to be rarely practically identifiable without high-frequency, low-noise data [25]. Throughout, we distinguish, following [33], between *structural* non-identifiability, a property of the model and the observation function that persists for noise-free data sampled continuously, and *practical* non-identifiability, which concerns the finite sampling design and the measurement noise actually assumed.

Against this backdrop, two issues remain under-addressed, and together they define the gap this paper targets. First, the fractional glucose–insulin literature often uses the term "identifiability" while in fact establishing well-posedness: existence, uniqueness, positivity, boundedness and continuous (Lipschitz) dependence of the solution on the parameters [5, 8]. Continuous dependence guarantees that small parameter perturbations produce small trajectory changes; it does not guarantee the converse—that the observed trajectory determines the parameters. In particular, the fractional orders are almost always fixed or swept as chosen constants rather than estimated jointly with the kinetic constants, so the question "are the fractional orders identifiable from IVGTT data?" has, to our knowledge, not been posed. Second, identifiability verdicts are usually drawn on top of low-order solvers—predictor–corrector, successive approximation, or truncated-series methods—and it is rarely checked whether they are sensitive to the accuracy of the forward computation. Two features of the enriched model make this check relevant: the non-smooth threshold secretion term $[G - h]_+$, which reduces the forcing to C^0 regularity at the switching instant, and the jump of the forcing at the delay breakpoints, which, for fractional orders, generates weakly singular behaviour of the solution there. Existing solvers for these fractional glucose–insulin systems are predominantly transform-based or low-order [3, 13], and none is tailored to the non-smooth, delayed setting; the spectral ingredients we combine (operational matrices and the method of steps) are individually standard, our contribution being their assembly and its use for a numerically controlled identifiability study.

The present work addresses both issues. Our contributions are as follows.

Uncorrected Proof

(1) We assemble a literature-grounded four-state glucose–insulin–glucagon minimal model with component-wise Caputo derivatives, a discrete secretion delay, and non-smooth threshold secretion, each term traceable to established formulations [7, 9, 27, 28, 35], and we write it in a dimensionally consistent form in which no parameter unit depends on a fractional order. We treat the model not as a validated physiological discovery but as the "maximally enriched" object the field is implicitly building toward.
(2) We solve it with a hybrid Chebyshev–Legendre operational-matrix collocation scheme in which the delay-induced breakpoints and the threshold-switching instants are imposed as subdomain interfaces, with geometric grading after the breakpoints at which the forcing jumps and an exact treatment of the weakly singular memory integral at interface nodes.
(3) On this solver we perform a practical identifiability analysis via the singular value decomposition of the noise-whitened sensitivity matrix, in which the fractional orders are treated as free parameters.
(4) We benchmark accuracy against computing time against a fractional Adams–Bashforth–Moulton (predictor–corrector) scheme [4, 11], and we quantify how much of the identifiability verdict depends on the accuracy and on the treatment of the delay in the forward solver.
(5) We determine the identifiable parameter subset under the assumed design and identify which supplementary measurement (a glucagon assay) restores identifiability of the counter-regulatory block.

The central message is cautionary: biologically motivated enrichment of the minimal model can add degrees of freedom that the standard data cannot resolve, and an identifiability verdict should be reported together with evidence that it is not an artefact of the forward computation.

The remainder of the paper is organised as follows. Section 2 presents the model, its history-function initialisation, and its nondimensional form. Section 3 develops the domain-decomposed collocation scheme, including all implementation parameters and the convergence of the nonlinear iteration. Section 4 reports the numerical benchmarks. Section 5 presents the identifiability analysis. Section 6 discusses the findings and Section 7 concludes.

Uncorrected Proof

2. The delayed fractional-order glucose–insulin–glucagon model

2.1. **Governing equations.** Let $G(t)$ denote plasma glucose concentration, $I(t)$ plasma insulin, $X(t)$ the remote insulin-action variable, and $Y(t)$ plasma glucagon, with t measured in minutes. For component-wise fractional orders $\alpha_G, \alpha_X, \alpha_I, \alpha_Y \in (0,1]$ and a fixed reference time $t_c > 0$ we consider, for $t \in (0, t_f]$,

$$t_c^{\alpha_G - 1}\, {}^{C}D_t^{\alpha_G} G(t) = -p_1\big(G(t) - G_b\big) - X(t)\, G(t) + \omega\big(Y(t) - Y_b\big) + \mathcal{I}_G(t), \tag{2.1a}$$

$$t_c^{\alpha_X - 1}\, {}^{C}D_t^{\alpha_X} X(t) = -p_2\, X(t) + p_3\big(I(t) - I_b\big), \tag{2.1b}$$

$$t_c^{\alpha_I - 1}\, {}^{C}D_t^{\alpha_I} I(t) = \gamma\,[G(t-\tau) - h]_+ - n\big(I(t) - I_b\big) + \mathcal{I}_I(t), \tag{2.1c}$$

$$t_c^{\alpha_Y - 1}\, {}^{C}D_t^{\alpha_Y} Y(t) = -p_4\, Y(t) + \sigma\,[h_Y - G(t-\tau)]_+, \tag{2.1d}$$

where ${}^{C}D_t^{\alpha}$ is the Caputo fractional derivative of order α,

$${}^{C}D_t^{\alpha} u(t) = \frac{1}{\Gamma(1-\alpha)} \int_0^t (t-s)^{-\alpha} u'(s)\, \mathrm{d}s, \qquad 0 < \alpha \le 1, \tag{2.2}$$

and $[z]_+ = \max\{z, 0\}$ denotes the positive part. Equations (2.1a)–(2.1b) are the fractional Bergman core: glucose is cleared by insulin-independent effectiveness p_1 toward its basal level G_b and by the remote insulin action X, while X is driven by suprabasal insulin with transfer coefficient p_3 and decays at rate p_2 [9, 30]. Equation (2.1c) is the pancreatic secretion balance: β-cells respond to glucose in excess of the threshold h, sensed with delay τ, and plasma insulin is cleared at rate n. Equation (2.1d) is the glucagon compartment: a single plasma pool with first-order clearance p_4 and α-cell secretion that decreases linearly as glucose rises and vanishes above the suppression level h_Y, again sensed with delay τ; glucagon raises hepatic glucose output in (2.1a) through the coupling ω, in opposition to insulin [7, 27, 28, 35]. The exogenous terms $\mathcal{I}_G, \mathcal{I}_I$ represent glucose and insulin inputs.

Dimensional consistency. The factor $t_c^{\alpha-1}$ is essential. Since ${}^{C}D_t^{\alpha}u$ carries the units of u per (time)$^{\alpha}$, the left-hand side of each equation in (2.1) has the units of the corresponding state per minute *for every order* α. Consequently every rate constant has a fixed physical dimension that does not depend on any fractional order (Table 1); in particular X and p_1 are both measured in min^{-1}, so that the terms $p_1(G-G_b)$ and XG in (2.1a) are commensurable, and p_3 is measured in $(\mathrm{mU\,L^{-1}})^{-1}\mathrm{min}^{-2}$ irrespective of α_G and α_X. The reference time is a fixed modelling constant, not an estimated parameter; we take $t_c = 1\,\mathrm{min}$, the time unit of the sampling protocol, so that numerical parameter values in minutes coincide with those of the usual formulation. The factor $t_c^{\alpha-1}$ is the standard device for keeping fractional models dimensionally homogeneous; without it, changing a fractional order would implicitly change the physical dimension of the rate constants in that equation, which is untenable when the orders are themselves estimated. As a check, we solved the model with time expressed in seconds ($t_c = 60\,\mathrm{s}$, all rates rescaled accordingly) and recovered the solution in minutes to a relative difference of 1.6×10^{-15}; omitting the factor $t_c^{\alpha-1}$ in the same experiment changes the solution by 29%, which exhibits the unit dependence of the uncorrected formulation.

Remark 2.1 (Threshold nonlinearity)**.** The secretion terms $[G(t-\tau)-h]_+$ and $[h_Y - G(t-\tau)]_+$ follow the original Bergman formulation of glucose-triggered secretion. They render the right-hand side only Lipschitz continuous at any instant $t^\star$ where $G(t^\star-\tau)=h$ or $G(t^\star-\tau)=h_Y$. The resulting loss of smoothness of the solution at $t^\star$ is weakened, but not removed, by the fractional integration, and it limits the accuracy of any global polynomial approximation across $t^\star$. The switching instants are therefore placed on subdomain interfaces (Section 3); Section 4.2 shows that this improves the accuracy by several orders of magnitude. A smooth Hill-type alternative $G^2/(\kappa+G^2)$ is available [24]; we retain the threshold form because it is the standard minimal-model choice.

2.2. **History function and IVGTT initialisation.** Because (2.1) contains the discrete delay τ, the state on $[-\tau,0]$ must be prescribed by a history function rather than a single initial value,

$$(G,X,I,Y)(t) = (\varphi_G,\varphi_X,\varphi_I,\varphi_Y)(t), \qquad t\in[-\tau,0]. \tag{2.3}$$

For an IVGTT we take the subject at rest on $[-\tau,0)$, i.e. $\varphi_G\equiv G_b$, $\varphi_X\equiv 0$, $\varphi_I\equiv I_b$, $\varphi_Y\equiv Y_b$, and impose the glucose bolus as the jump condition

$$G(0^+) = G_0 > G_b, \qquad X(0^+)=0, \qquad I(0^+)=I_b, \qquad Y(0^+)=Y_b, \tag{2.4}$$

with $\mathcal{I}_G\equiv\mathcal{I}_I\equiv 0$ for $t>0$. Consistency of (2.3)–(2.4) with (2.2) requires the lower terminal of the Caputo integral to be fixed at $t=0$, so that the memory kernel acts on the post-bolus trajectory. The resting history is an equilibrium of (2.1) provided $h\ge G_b$ (no insulin secretion at basal glucose) and $p_4Y_b=\sigma(h_Y-G_b)$ (basal glucagon secretion balances clearance); the nominal values in Table 1 satisfy both conditions, and the second one fixes $h_Y = G_b + p_4Y_b/\sigma$. Standard results for Caputo fractional delay differential equations with a Lipschitz right-hand side and a bounded history give existence and uniqueness of a continuous solution on $[0,t_f]$; we use this only as well-posedness and do not conflate it with identifiability.

2.3. **Parameters.** Table 1 lists the states and parameters with their roles, units and nominal values. The model carries eighteen scalar unknowns: six kinetic constants (p_1,p_2,p_3,n,γ,h), three basal levels (G_b,I_b,Y_b), four glucagon-block constants (p_4,ω,σ,h_Y), the delay τ, and the four fractional orders $(\alpha_G,\alpha_X,\alpha_I,\alpha_Y)$. Only G and I are observed in a standard IVGTT; X and Y are latent. The basal levels G_b, I_b are directly measurable before the bolus; we nonetheless retain them in the estimated set for completeness. The glucose–insulin constants lie within the ranges reported for the classical minimal model [9, 30]; the glucagon-block constants are illustrative. The operating point is thus physiologically plausible, though not fitted to a specific cohort.

2.4. **Nondimensional form.** Let $\bar t = t/t_c$ and $\bar\tau=\tau/t_c$, and introduce the dimensionless states

$$g=\frac{G-G_b}{G_b}, \qquad \xi = t_cX, \qquad i=\frac{I-I_b}{I_b}, \qquad y=\frac{Y-Y_b}{Y_b}. \tag{2.5}$$

Uncorrected Proof

TABLE 1. States and parameters of model (2.1). Because of the factor $t_c^{\alpha-1}$ in (2.1), no unit depends on a fractional order; the units therefore remain valid when the orders are estimated. The nominal values are illustrative (not fitted to a cohort) and are those used in the accompanying script; h_Y follows from the basal balance $p_4 Y_b = \sigma(h_Y - G_b)$.

Symbol	Meaning	Unit	Nominal value
G	plasma glucose (observed)	$\mathrm{mg\,dL^{-1}}$	$G(0^+) = G_0 = 280$
I	plasma insulin (observed)	$\mathrm{mU\,L^{-1}}$	$I(0^+) = I_b$
X	remote insulin action (latent)	$\mathrm{min^{-1}}$	$X(0^+) = 0$
Y	plasma glucagon (latent; observed with assay)	$\mathrm{pg\,mL^{-1}}$	$Y(0^+) = Y_b$
p_1	glucose effectiveness	$\mathrm{min^{-1}}$	0.028
p_2	insulin-action decay	$\mathrm{min^{-1}}$	0.025
p_3	insulin→action transfer	$(\mathrm{mU\,L^{-1}})^{-1}\mathrm{min^{-2}}$	1.3×10^{-5}
n	insulin clearance	$\mathrm{min^{-1}}$	0.09
γ	β-cell responsivity	$\mathrm{mU\,L^{-1}\,(mg\,dL^{-1})^{-1}\,min^{-1}}$	0.0045
h	insulin-secretion threshold	$\mathrm{mg\,dL^{-1}}$	100
p_4	glucagon clearance	$\mathrm{min^{-1}}$	0.05
ω	glucagon→glucose coupling	$\mathrm{mg\,dL^{-1}\,(pg\,mL^{-1})^{-1}\,min^{-1}}$	0.02
σ	α-cell responsivity	$\mathrm{pg\,mL^{-1}\,(mg\,dL^{-1})^{-1}\,min^{-1}}$	0.03
h_Y	glucagon-suppression level	$\mathrm{mg\,dL^{-1}}$	206.67
τ	secretion delay	min	8
$G_b,\ I_b,\ Y_b$	basal levels	as G, I, Y	90, 10, 70
$\alpha_G, \alpha_X, \alpha_I, \alpha_Y$	fractional orders	—	0.95 each
t_c	reference time (fixed, not estimated)	min	1

Under $t = t_c\bar{t}$ the Caputo operator scales as ${}^{C}D_t^{\alpha}u = t_c^{-\alpha}\,{}^{C}D_{\bar{t}}^{\alpha}u$, so that $t_c^{\alpha-1}\,{}^{C}D_t^{\alpha}u = t_c^{-1}\,{}^{C}D_{\bar{t}}^{\alpha}u$ for every order. Since the Caputo derivative annihilates constants, (2.1) becomes (for $t > 0$, without exogenous inputs)

$$ {}^{C}D_{\bar{t}}^{\alpha_G} g = -k_1\, g - \xi\,(1+g) + k_\omega\, y, \tag{2.6a} $$

$$ {}^{C}D_{\bar{t}}^{\alpha_X} \xi = -k_2\, \xi + k_3\, i, \tag{2.6b} $$

$$ {}^{C}D_{\bar{t}}^{\alpha_I} i = k_\gamma \left[1 + g(\bar{t}-\bar{\tau}) - \eta\right]_+ - k_n\, i, \tag{2.6c} $$

$$ {}^{C}D_{\bar{t}}^{\alpha_Y} y = -k_4\,(1+y) + k_\sigma \left[\eta_Y - 1 - g(\bar{t}-\bar{\tau})\right]_+, \tag{2.6d} $$

with the dimensionless groups

$$ \begin{aligned} &k_1 = t_c p_1, \quad k_2 = t_c p_2, \quad k_3 = t_c^2 p_3 I_b, \quad k_n = t_c n, \quad k_\gamma = \frac{t_c \gamma G_b}{I_b}, \\ &k_4 = t_c p_4, \quad k_\omega = \frac{t_c \omega Y_b}{G_b}, \quad k_\sigma = \frac{t_c \sigma G_b}{Y_b}, \quad \eta = \frac{h}{G_b}, \quad \eta_Y = \frac{h_Y}{G_b}, \end{aligned} \tag{2.7} $$

history $g = \xi = i = y = 0$ on $[-\bar{\tau}, 0)$ and initial values $g(0^+) = (G_0 - G_b)/G_b$, $\xi(0^+) = i(0^+) = y(0^+) = 0$. Every group in (2.7) is dimensionless for all fractional orders. The nondimensional system (2.6) is the system actually discretised in Section 3; transforming its solution back through (2.5) reproduces a direct solution of the dimensional system (2.1) (same predictor–corrector scheme, $\alpha_\bullet = 0.95$) to a relative difference of 7×10^{-16}.

Remark 2.2 (Fractional orders are entangled with the time scale)**.** The reference time enters (2.1) only through the factor $t_c^{1-\alpha}$ multiplying each right-hand side. Replacing t_c by λt_c is therefore equivalent to multiplying every rate constant in the equation of order α by $\lambda^{1-\alpha}$. For $\alpha < 1$ the order thus acts partly as a time-scale parameter: a change in α alters the effective rates in the same way as a change in the rate constants, and the two can compensate each other over a finite observation window. This algebraic entanglement is one concrete mechanism by which an order

Uncorrected Proof

and a rate can trade off against each other; it foreshadows the parameter-trade-off directions examined in Section 5. In the integer-order case the factor equals one and the classical minimal model is recovered.

3. Domain-decomposed spectral collocation

We solve the nondimensional system (2.6) by a four-layer strategy: (i) the method of steps removes the delay by turning it into known forcing; (ii) domain decomposition places the delay breakpoints and any threshold crossings on subdomain interfaces, with geometric grading after the breakpoints; (iii) on each subdomain a hybrid Chebyshev–Legendre collocation based on the fractional-integral operational matrix is applied; (iv) the nonlinearity is resolved by fixed-point (Picard) iteration. All numerical parameters are listed in Table 2. In this section t denotes the dimensionless time $\bar{t}$.

3.1. **Method of steps.** The discrete delay partitions time into the primary breakpoints $0, \tau, 2\tau, \dots$. On the step $[k\tau, (k+1)\tau]$ the delayed argument $t-\tau$ lies in $[(k-1)\tau, k\tau]$, already solved; on the first step it lies in the history interval $[-\tau, 0]$. The delayed glucose is therefore known data on each step, and (2.6) reduces to a sequence of fractional (delay-free) problems.

3.2. **Breakpoints, regularity and interfaces.** Three mechanisms reduce the regularity of the solution. (a) At $t=0$ the Caputo solution behaves as $u(t)-u(0) \sim c\,t^{\alpha}$. (b) The bolus makes G discontinuous at $t=0$, so the delayed forcing $g(t-\tau)$ jumps at $t=\tau$. For $\alpha<1$ a jump of the forcing at $t=\tau$ produces a term proportional to $(t-\tau)^{\alpha}$ in the solution; this singularity is of the same type as that at the origin and, unlike in the integer-order case, is not confined to a corner of the derivative. Weaker singularities of the form $(t-k\tau)^{k\alpha}$ propagate to later breakpoints. (c) Whenever the delayed glucose crosses a secretion threshold, $G(t^{\star}-\tau)=h$ or h_Y, the right-hand side has a corner at $t^{\star}$.

Accordingly, the subdomain interfaces are (i) the primary breakpoints $k\tau$; (ii) J geometrically graded points $k\tau+\tau q^{j}$, $j=J,\dots,1$, with ratio $q=1/4$, after each primary breakpoint; and (iii) every threshold-crossing instant $t^{\star}$, followed by J graded points $t^{\star}+(B-t^{\star})q^{j}$ inside the subdomain $[A,B]$ in which it occurs. Because the delayed glucose is known on each step, threshold crossings are located before the subdomain is solved: the functions $1+g(t-\tau)-\eta$ and $\eta_Y-1-g(t-\tau)$ are evaluated on 401 equispaced points of $[A,B]$ from the stored interpolants, and each sign change is refined by Brent's method to an absolute tolerance of 10^{-14}. Crossings closer than 10^{-8} to an existing interface are ignored. On every subdomain the right-hand side of (2.6) is then continuous, and on subdomains not adjacent to a breakpoint it is infinitely differentiable; the singular terms (a)–(c) are confined to subdomains whose length decreases geometrically toward the breakpoint. This is the regularity on which the accuracy argument of Section 3.4 relies; we do not require analyticity.

3.3. **Fractional-integral collocation on a subdomain.** On a subdomain $[A,B]$, integrating the Caputo form (lower terminal fixed at 0) gives, for each state u with order α and right-hand side f,

$$u(t)=u(0)+\underbrace{\frac{1}{\Gamma(\alpha)}\int_{0}^{A}(t-s)^{\alpha-1}f(s)\,\mathrm{d}s}_{\text{memory tail (known)}}+\underbrace{\frac{1}{\Gamma(\alpha)}\int_{A}^{t}(t-s)^{\alpha-1}f(s)\,\mathrm{d}s}_{\text{local}}, \tag{3.1}$$

where $u(0)$ is the global initial value. Continuity across interfaces is automatic in (3.1); it need not be imposed separately.

Hybrid nodes and matrices. We interpolate on the Chebyshev–Gauss–Lobatto (CGL) nodes $\{t_m\}_{m=0}^{M}$ of $[A,B]$ in barycentric form. Writing f through its nodal values on the Lagrange basis $\{\ell_m\}$, the local term becomes a matrix $\mathbf{W}^{(\alpha)}$ acting on the nodal values of f,

$$W_{nm}^{(\alpha)}=\frac{1}{\Gamma(\alpha)}\int_{A}^{t_n}(t_n-s)^{\alpha-1}\ell_m(s)\,\mathrm{d}s=\frac{(t_n-A)^{\alpha}}{2^{\alpha}\Gamma(\alpha)}\sum_{q=1}^{N_J}\varpi_q\,\ell_m\Big(t_n-\tfrac{t_n-A}{2}(1+x_q)\Big), \tag{3.2}$$

where $\{x_q,\varpi_q\}$ is the N_J-point Gauss–Jacobi rule for the weight $(1+x)^{\alpha-1}$ on $[-1,1]$. Since ℓ_m composed with the affine map is a polynomial of degree M in x and the rule is exact for polynomials of degree $2N_J-1$, formula

Uncorrected Proof

(3.2) is exact (up to rounding) whenever $N_J \geq \lceil (M+1)/2 \rceil$. We use $N_J = 40$, which satisfies this condition for all $M \leq 79$ and therefore for every degree used in this paper ($M \leq 48$). This is the shifted operational matrix of the Caputo fractional integral; the Jacobi-based quadrature supplies the operator while the Chebyshev nodes supply stable interpolation—hence "hybrid Chebyshev–Legendre".

Memory tail. The tail is the sum over all previously solved subdomains $S = [a, b]$, $b \leq A$, of $\Gamma(\alpha)^{-1} \int_a^b (t_n - s)^{\alpha-1} f_S(s)\, \mathrm{d}s$, where f_S is the stored degree-M interpolant of f on S. Three cases are distinguished according to the distance $d = t_n - b \geq 0$ between the node and the subdomain.

- $d \geq 0.1\,(b-a)$: the kernel is analytic on S and the integral is evaluated by 32-point Gauss–Legendre quadrature; the Bernstein-ellipse estimate for this distance bounds the quadrature error by approximately 10^{-17} relative to the integrand scale.
- $d = 0$, i.e. the interface node $t_0 = A = b$ and the subdomain S immediately to its left: here the kernel $(A - s)^{\alpha-1}$ has the weak endpoint singularity of the fractional integral. Writing $s = \frac{a+b}{2} + \frac{b-a}{2} x$, the integral equals $\left(\frac{b-a}{2}\right)^{\alpha} \int_{-1}^{1} (1-x)^{\alpha-1} f_S(s(x))\, \mathrm{d}x$, which is evaluated *exactly* for the polynomial f_S by the 40-point Gauss–Jacobi rule for the weight $(1-x)^{\alpha-1}$.
- $0 < d < 0.1\,(b-a)$: the kernel is smooth but nearly singular at $s = b$; the integral is evaluated by adaptive Gauss–Kronrod quadrature (`scipy.integrate.quad_vec`) with absolute and relative tolerances 10^{-15} and 10^{-13}. The largest error estimate returned in the computations reported below is 6×10^{-14}.

The second case is precisely the situation of the interface node $t_n = A$, at which a standard Gauss–Legendre rule converges only algebraically. If this node is instead treated by 24-point Gauss–Legendre quadrature, the attainable accuracy is limited to about 10^{-5} (Section 4.1).

Collocation system and Picard iteration. Enforcing (3.1) at the CGL nodes gives, per state,

$$u(t_n) = u(0) + \mathrm{hist}(t_n) + \sum_{m=0}^{M} W_{nm}^{(\alpha)}\, f(t_m), \qquad n = 0, \ldots, M, \tag{3.3}$$

in which $f(t_m)$ depends on the unknown nodal states (linearly and, through $\xi(1+g)$, quadratically) and on the known delayed glucose. Writing (3.3) for the four states as $\mathbf{U} = \mathcal{P}(\mathbf{U}) := \mathbf{u}_0 + \mathbf{h} + \mathbf{W}\,\mathbf{F}(\mathbf{U})$, the Picard iteration is $\mathbf{U}^{(k+1)} = \mathcal{P}(\mathbf{U}^{(k)})$ without relaxation. The initial iterate on every subdomain is the constant state equal to the solution at its left endpoint A (on the first subdomain, the post-bolus initial value). The iteration stops when $\|\mathbf{U}^{(k+1)} - \mathbf{U}^{(k)}\|_\infty < 10^{-14}$ (dimensionless states), with at most 300 iterations; this limit was never reached. At the right-end node the delayed glucose is taken as the left limit and elsewhere as the right limit, so that a jump of the delayed forcing at an interface is attributed consistently to the subdomain on each side.

Convergence of the Picard iteration. The continuous problem underlying (3.3) is a Volterra integral equation with a weakly singular kernel. For such equations, if $\mathbf{F}$ is Lipschitz with constant L on a set containing the iterates, the Picard iterates satisfy $\|\mathbf{U}^{(k)} - \mathbf{U}\| \leq C\,(L\,\ell^{\alpha})^k / \Gamma(k\alpha + 1)$ on a subdomain of length ℓ, so the iteration converges for every subdomain length; this is the standard argument behind existence for fractional differential equations. For the discrete map, a sufficient condition for contraction in the maximum norm is

$$q := L \max_c \left\| \mathbf{W}^{(\alpha_c)} \right\|_\infty < 1, \qquad \left\| \mathbf{W}^{(\alpha)} \right\|_\infty \leq \frac{\Lambda_M\, \ell^{\alpha}}{\Gamma(\alpha + 1)}, \tag{3.4}$$

with Λ_M the Lebesgue constant of the CGL nodes. Condition (3.4) is sufficient but pessimistic, because it ignores the Volterra structure of $\mathbf{W}$; it can always be enforced by shortening the subdomains. The quantity that governs local convergence is the spectral radius ρ of the Jacobian $\partial\mathcal{P}/\partial\mathbf{U} = \mathbf{W}\,\partial\mathbf{F}/\partial\mathbf{U}$ at the fixed point, since the iteration converges locally if and only if $\rho < 1$, with asymptotic rate ρ. We compute ρ for every subdomain. For all configurations reported in this paper $\rho \leq 0.039$, the observed ratio of successive updates is at most 0.10, and the iteration converges in 4 to 15 steps (Table 2).

The steps carried out on one subdomain $[A, B]$ are summarised in Algorithm 1.

Uncorrected Proof

TABLE 2. Implementation parameters of the collocation solver and observed behaviour of the Picard iteration for the nominal parameters (Table 1). ρ: spectral radius of $\mathbf{W}\,\partial\mathbf{F}/\partial\mathbf{U}$ at the converged solution, maximised over subdomains.

Item	Value
Local operational matrix (3.2)	Gauss–Jacobi, $N_J = 40$ nodes, weight $(1+x)^{\alpha-1}$ (exact for $M \le 79$)
Memory tail, $d \ge 0.1(b-a)$	Gauss–Legendre, 32 nodes
Memory tail, $d = 0$ (interface node)	Gauss–Jacobi, 40 nodes, weight $(1-x)^{\alpha-1}$ (exact)
Memory tail, $0 < d < 0.1(b-a)$	adaptive Gauss–Kronrod, tolerances 10^{-15} (abs), 10^{-13} (rel)
Grading after breakpoints	ratio $q = 1/4$, $J = 4$ points (unless stated otherwise)
Threshold detection	401-point sign scan of the known delayed glucose, Brent refinement to 10^{-14}
Picard iteration	no relaxation; initial iterate = state at left endpoint; tolerance 10^{-14}; max. 300
Observed Picard iterations	4–15 per subdomain; $\rho \le 0.039$; update ratio ≤ 0.10

Algorithm 1 Solution on one subdomain $[A, B]$.

1: Locate threshold roots $t^\star \in (A, B)$ of the known delayed glucose; if any, split $[A, B]$ at $t^\star$ (with grading) and process the pieces in order.
2: Build the CGL nodes and, for each order α_c, the matrix $\mathbf{W}^{(\alpha_c)}$ from (3.2).
3: Compute the memory tail hist(t_n) from the stored subdomains as described above.
4: Initialise $\mathbf{U}$ with the state at A and iterate (3.3) to convergence.
5: Store the nodal $\mathbf{U}$ and $\mathbf{F}$; advance to the next subdomain.

3.4. **Accuracy expectation.** On a subdomain on which f is infinitely differentiable, the interpolation error of f, and hence the local error, decreases faster than any power of M. On subdomains adjacent to a breakpoint the terms $(t-k\tau)^\alpha$ of Section 3.2 restrict polynomial approximation to algebraic convergence in M. Geometric grading confines these terms to subdomains whose length, and therefore whose contribution to the error, decreases geometrically; this is the mechanism of *hp*-type approximation of weakly singular Volterra problems. Without grading, the global error is limited by the singular behaviour at the first breakpoint at which the forcing jumps. Section 4 quantifies both regimes.

4. NUMERICAL VALIDATION AND BENCHMARK

We verify the solver on the nominal parameter set (Table 1) over the horizon $t_f = 16 = 2\tau$, which contains the delay breakpoint $t = \tau$ at which the delayed forcing jumps. The error measure is

$$E = \max_{c\in\{g,\xi,i,y\}} \frac{\max_k |u_c(t_k) - u_c^{\mathrm{ref}}(t_k)|}{\max_k |u_c^{\mathrm{ref}}(t_k)|}, \tag{4.1}$$

taken over 120 equispaced times $t_k \in [0.5, 16]$, i.e. the largest error of any state relative to the magnitude of its excursion. The reference solution is the graded collocation solution with $M = 40$, $J = 10$; it agrees with an independent computation with $M = 48$, $J = 12$ to 6×10^{-16}, and the fractional predictor–corrector solutions converge to it at first order as the step is refined (Figure 1(C)).

Independent checks. Before the benchmark, four checks were passed. (i) For $\alpha_\bullet = 1$ the scheme reproduces a method-of-steps solution computed with an eighth-order Dormand–Prince integrator (relative tolerance 10^{-13}) to 2.2×10^{-13} over $[0, 30]$ with $M = 16$. (ii) For the scalar problem ${}^{C}D^{0.8}u = -0.3u + 0.5\,H(t-4)$, $u(0) = 1$, whose exact solution is $u = E_{0.8}(-0.3t^{0.8}) + 0.5(t-4)^{0.8}E_{0.8,1.8}(-0.3(t-4)^{0.8})H(t-4)$, the error at $M = 24$ is 1.2×10^{-3} with an interface at the jump only and 4.2×10^{-7} with grading $J = 4$; this isolates the $(t-\tau)^\alpha$ singularity induced by a jump of the forcing. (iii) The nondimensionalisation and unit-invariance checks of Section 2 are passed at the level of rounding. (iv) The qualitative IVGTT response is correct: glucose returns toward basal, insulin rises, and glucagon secretion is suppressed while glucose exceeds h_Y.

Uncorrected Proof

TABLE 3. Accuracy and cost of the forward solvers on $[0, 16]$. E: error (4.1) against the reference solution. Nodes: collocation nodes per state (spectral); steps: time steps (PECE). CPU: median over repeated runs (Section 4.1). Legacy interface quadrature: 24-point Gauss–Legendre rule at the interface node in place of the exact Gauss–Jacobi rule.

Scheme	Resolution	Nodes/steps	E	CPU (s)
single domain	$M = 8$	9	3.7×10^{-1}	0.004
	$M = 16$	17	1.8×10^{-1}	0.006
	$M = 24$	25	1.2×10^{-1}	0.008
method of steps (interfaces at $0, \tau, 2\tau$)	$M = 8$	18	7.0×10^{-4}	0.022
	$M = 12$	26	2.9×10^{-4}	0.024
	$M = 16$	34	1.3×10^{-4}	0.026
	$M = 20$	42	5.9×10^{-5}	0.030
	$M = 24$	50	5.0×10^{-5}	0.031
method of steps, origin graded ($J = 4$)	$M = 8$	54	7.0×10^{-4}	0.041
	$M = 16$	102	1.3×10^{-4}	0.110
	$M = 24$	150	5.0×10^{-5}	0.122
method of steps, graded at 0 and τ ($J = 4$)	$M = 4$	50	5.4×10^{-5}	0.134
	$M = 6$	70	2.5×10^{-6}	0.139
	$M = 8$	90	1.5×10^{-7}	0.139
	$M = 10$	110	1.1×10^{-8}	0.239
	$M = 12$	130	8.6×10^{-10}	0.245
	$M = 16$	170	7.0×10^{-12}	0.258
as above, legacy interface quadrature	$M = 8$	90	1.8×10^{-5}	0.082
	$M = 20$	210	1.3×10^{-5}	0.103
fractional PECE (interpolated delay)	$h = 0.08$	200	1.5×10^{-2}	0.020
	$h = 0.04$	400	7.7×10^{-3}	0.076
	$h = 0.02$	800	3.6×10^{-3}	0.116
	$h = 0.01$	1600	2.1×10^{-3}	0.321
	$h = 0.005$	3200	9.2×10^{-4}	1.198

Uncorrected Proof

4.1. **Effect of domain decomposition, grading and interface quadrature.** Table 3 and Figure 1 compare a single global spectral domain, the method of steps with interfaces at the primary breakpoints only, the method of steps with grading at the origin only, the fully graded scheme, and the fractional predictor–corrector (PECE) method of Diethelm, Ford and Freed [11] with the delayed term obtained by linear interpolation. CPU times are medians over seven runs for the collocation schemes and three runs for PECE, measured on a single core of an Intel Xeon processor at 2.80 GHz (Linux, Python 3.11, NumPy 2.4, SciPy 1.17); they are indicative and hardware dependent. We report the number of collocation nodes per state for the spectral schemes and the number of time steps for PECE; these are resolution measures, not equivalent measures of work, and the comparison of work is made through CPU time in Figure 1(A). The following findings emerge.

(1) *Interfaces at the delay breakpoints are indispensable.* A single global expansion, in which the jump of the delayed forcing at $t = \tau$ falls inside the domain, attains only $E = 1.2 \times 10^{-1}$ at $M = 24$. Placing τ on an interface reduces the error to 5.0×10^{-5} at the same degree.

(2) *The limiting singularity is at the delay breakpoint, not at the origin.* Without grading, the method of steps converges only algebraically. Grading at the origin alone leaves the error unchanged (relative change below 1×10^{-5} for every M), because the dominant error comes from the term $(t - \tau)^{\alpha}$ generated by the jump of the delayed forcing (Section 3.2). Grading after both 0 and τ restores rapid convergence: E decreases from 5.4×10^{-5} at $M = 4$ to 7.0×10^{-12} at $M = 16$ (Figure 1(B)).

(3) *The interface quadrature matters.* With a 24-point Gauss–Legendre treatment of the interface node (the legacy variant in Table 3 and Figure 1(B)), the graded scheme stagnates at $E \approx 1.3 \times 10^{-5}$ irrespective of M; the exact Gauss–Jacobi treatment of Section 3 removes this floor.
(4) *Efficiency.* The PECE error decreases at first order in h, as expected for a forcing that is discontinuous at $t = \tau$; $h = 0.005$ (3200 steps) gives $E = 9.2 \times 10^{-4}$ in 1.20 s. The ungraded method of steps reaches a smaller error, 7.0×10^{-4}, with $M = 8$ in 0.022 s, and the graded scheme reaches 2.5×10^{-6} in 0.14 s. On the error–CPU diagram (Figure 1(A)), the ungraded method of steps for moderate accuracy and the graded scheme for high accuracy require less CPU time than PECE for every accuracy target below about 5×10^{-3}, and the gap widens as the target is tightened; for targets near 10^{-2} the costs are comparable. We emphasise that the comparison concerns this problem class, in which the breakpoints are known in advance.

4.2. **The threshold interface.** To test the threshold-crossing interface directly we set the secretion threshold to a value that the glucose crosses on its descent ($h = 230\,\mathrm{mg\,dL^{-1}}$), so that the delayed glucose crosses it at an interior instant $t^\star$ (at $t^\star \approx 20.05$ min for $\alpha_\bullet = 0.95$), and integrate to $t_f = 40$ with $M = 12$ and $J = 4$, with and without the threshold interface. The interface is highly effective once the other error sources have been removed. For $\alpha_\bullet \in \{1, 0.99, 0.95, 0.90, 0.80\}$ the global error without the interface is between 3.2×10^{-5} and 5.7×10^{-4}, whereas with the interface it is between 8.8×10^{-13} and 6.7×10^{-9}; the improvement factor ranges from 4.8×10^{3} (at $\alpha_\bullet = 0.8$) to 6.5×10^{8} (at $\alpha_\bullet = 1$). The gain decreases as the order decreases, consistent with the smoothing effect of the fractional integral on the corner of the forcing, but it remains large. Restricted to a window of ± 1.5 min around $t^\star$ ($\alpha_\bullet = 0.95$), the error without the interface is 4.2×10^{-4} at $M = 12$ and with it 1.0×10^{-11}. This benefit is visible only when the interface-quadrature and delay-breakpoint errors are controlled; otherwise those errors dominate and mask it. The threshold interface is therefore part of the standard configuration used below.

These results establish the forward solver as accurate and reproducible, which is the prerequisite for the identifiability analysis: the verdicts of Section 5 rest on forward solutions whose error is controlled and quantified here.

5. Identifiability analysis

We now address the question the enrichment programme leaves open: given the verified forward solver, which of the eighteen parameters can standard IVGTT data determine?

5.1. **Sensitivity matrix, Fisher information and singular values.** Let $\theta \in \mathbb{R}^{18}$ collect the parameters and $\vartheta = \log\theta$ their logarithms, so that sensitivities are relative and unit-free. The observations are G and I (and, in Section 5.4, Y) at the fourteen times $t_k \in \{2, 3, 4, 5, 6, 8, 10, 12, 15, 18, 21, 24, 27, 30\}$ min, with independent Gaussian errors of standard deviation $\sigma_G = 2\,\mathrm{mg\,dL^{-1}}$, $\sigma_I = 0.5\,\mathrm{mU\,L^{-1}}$ and $\sigma_Y = 1.4\,\mathrm{pg\,mL^{-1}}$. The whitened sensitivity matrix is

$$\tilde{S} = W^{1/2} S, \qquad S_{(o,k),j} = \frac{\partial y_o(t_k;\theta)}{\partial \vartheta_j}, \qquad W = \mathrm{diag}(\sigma_o^{-2}), \tag{5.1}$$

and the Fisher information matrix is $F = \tilde{S}^\top \tilde{S} = S^\top W S$. The columns of S are computed by central differences with relative step $\delta = 10^{-3}$ on the collocation solution with $M = 12$, $J = 4$ and threshold interfaces, whose forward error on $[0, 30]$ is below 10^{-9} (Section 4); the breakpoints move with τ, so that $\partial/\partial\tau$ is a genuine derivative. Because F is formed from a Jacobian, it is positive semidefinite in exact arithmetic for *any* forward solver; its sign structure therefore carries no information about solver accuracy, and the smallest eigenvalues computed from F are dominated by rounding, since forming F squares the condition number. We therefore work with the singular value decomposition $\tilde{S} = U\Sigma V^\top$ directly, $\Sigma = \mathrm{diag}(s_1 \geq \cdots \geq s_{18})$, so that the eigenvalues of F are s_i^2 and its eigenvectors are the right singular vectors v_i.

The Cramér–Rao bound gives the standard deviation of the log-parameter combination $v_i^\top \vartheta$ as $1/s_i$. We call a direction *resolved above the noise* if $s_i > 1$, i.e. if the combination is determined to better than a factor of e, let k be the number of such directions, and define the participation of parameter j in the resolved subspace as $\pi_j = \sum_{i \leq k} V_{ji}^2 \in [0, 1]$. A parameter is classified as practically unidentifiable under the assumed design if $\pi_j < 1/2$, i.e. if more than half of its unit vector lies in the unresolved subspace. The threshold $s_i = 1$ and the cut $\pi_j = 1/2$ are

Uncorrected Proof

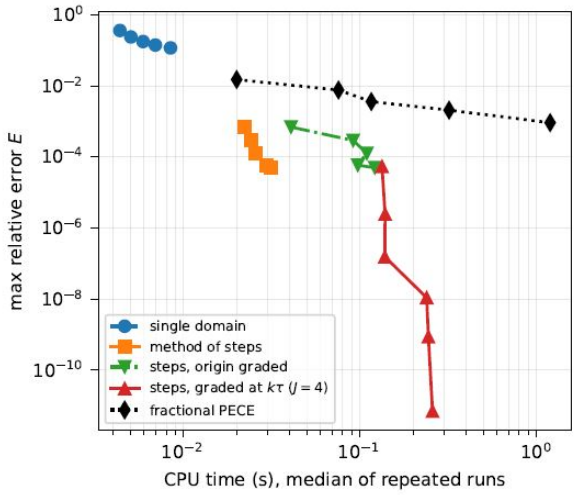

(A) Error versus CPU time.

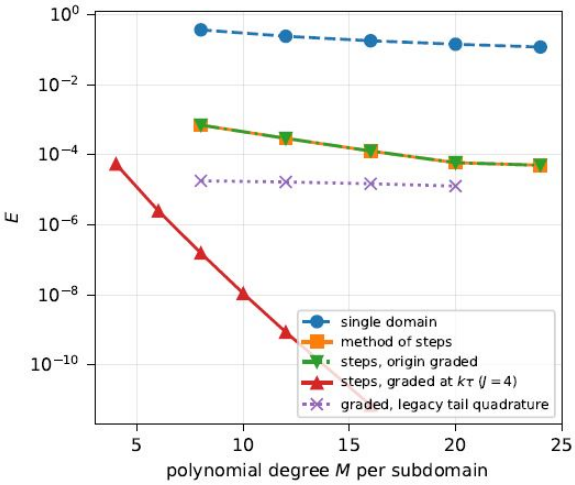

(B) Spectral resolution.

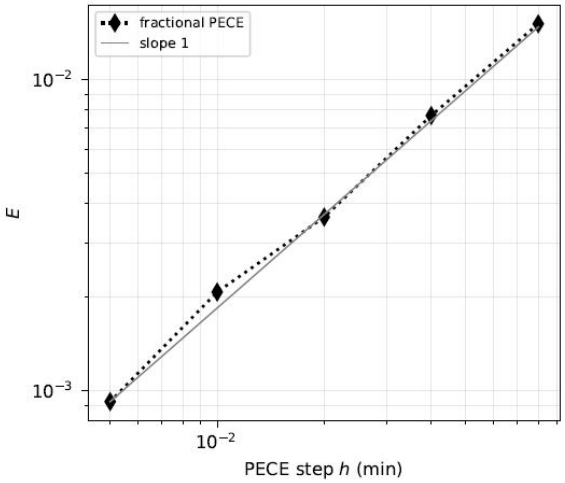

(C) PECE resolution.

FIGURE 1. (A) Maximum relative error E (4.1) versus CPU time (median of repeated runs) for the collocation variants and the fractional PECE method. (B) Error versus polynomial degree M per subdomain for the collocation variants, including the graded scheme with a 24-point Gauss–Legendre treatment of the interface node (legacy quadrature). (C) Error of PECE versus step size h, with a reference line of slope one.

conventions; the robustness of the classification to them is examined below. To separate genuine small singular values from numerical artefacts, the decomposition was repeated with $M = 16$. A singular value is regarded as numerically resolved if it changes by less than 1% between the two resolutions; all resolved values in fact change by at most 8.3×10^{-5} in relative terms, and unresolved values are not interpreted. Varying δ from 10^{-2} to 10^{-4} leaves k and the classification unchanged.

5.2. **Practical identifiability from glucose and insulin.** Figure 2(A) shows the singular values. The resolved singular values decrease from $s_1 = 248$ to 6.8×10^{-6}, a range of 7.6 decades; the spectrum is approximately evenly

spread on a logarithmic scale, which is the signature of a *sloppy* model in the sense of Gutenkunst et al. [21]. The smallest singular value, $s_{18} = 1.9 \times 10^{-11}$, is not numerically resolved (it changes by 35% between $M = 12$ and $M = 16$) and is consistent with zero; it is discussed below. Only $k = 8$ directions satisfy $s_i > 1$ ($s_8 = 1.62$, $s_9 = 0.32$). On the participation criterion, ten of the eighteen parameters are practically unidentifiable from glucose and insulin under this design (Table 4, Figure 2(B)): p_2, p_3, h, p_4, ω, σ, h_Y, G_b, Y_b, α_X. The identifiable complement is p_1, n, γ, τ, I_b, α_G, α_I, α_Y; the participation of α_Y, 0.55, is close to the cut and should be regarded as marginal.

Three groups can be distinguished by inspecting the unresolved singular vectors. (i) The insulin-action block: p_2, p_3 and the order α_X of the unobserved state X dominate the weakest resolved directions (s_{14}–s_{17}). (ii) The glucagon block $p_4, \omega, \sigma, h_Y, Y_b$, which acts on the observed glucose only through the coupling $\omega(Y - Y_b)$. (iii) Two parameters acting on observed states through affine combinations: as long as the delayed glucose exceeds h, the secretion term equals $\gamma G(t - \tau) - \gamma h$, and h trades off against γ and n (the direction of s_{11}); G_b enters through $p_1(G - G_b)$ and correlates with the glucagon block. In practice G_b is measured before the bolus and would be fixed.

A structural non-identifiability. The right singular vector of s_{18} is, to two digits, $(1, -1, 1)/\sqrt{3}$ in the coordinates $(\log Y_b, \log \omega, \log \sigma)$, with all other components negligible. This direction is an exact symmetry of the model. In the nondimensional system (2.6), the glucagon parameters enter only through $k_\omega = t_c \omega Y_b / G_b$, $k_\sigma = t_c \sigma G_b / Y_b$ and k_4, and the initial value $y(0^+) = 0$ does not involve Y_b. The transformation $(Y_b, \omega, \sigma) \mapsto (\lambda Y_b, \omega/\lambda, \lambda\sigma)$, $\lambda > 0$, leaves k_ω, k_σ and hence g, ξ, i and y unchanged, so the observed G and I are identical for every λ. The combination is therefore *structurally* non-identifiable from glucose and insulin, for any sampling schedule and any noise level; observing $Y = Y_b(1 + y)$ breaks the symmetry. All other losses reported here are *practical*: they reflect the finite sampling window and the assumed noise, and the associated singular values, although small, are numerically resolved.

TABLE 4. Participation π_j of each parameter in the subspace resolved above the noise ($s_i > 1$), from the singular value decomposition of the whitened sensitivity matrix; $\pi_j < 0.5$ (bold) denotes practical unidentifiability under the assumed design. Columns: glucose and insulin observed; glucose, insulin and glucagon observed. Number of resolved directions: $k = 8$ and $k = 13$.

Parameter	G, I	G, I, Y	Parameter	G, I	G, I, Y
p_1	0.86	0.92	h_Y	**0.06**	1.00
p_2	**0.00**	**0.00**	τ	1.00	1.00
p_3	**0.00**	**0.02**	G_b	**0.33**	0.63
n	0.87	0.87	I_b	1.00	1.00
γ	0.78	0.78	Y_b	**0.05**	1.00
h	**0.36**	**0.35**	α_G	0.99	1.00
p_4	**0.01**	1.00	α_X	**0.02**	**0.08**
ω	**0.13**	0.59	α_I	1.00	1.00
σ	**0.02**	0.76	α_Y	0.55	1.00

Uncorrected Proof

Robustness across operating points. To check that these counts are not specific to the nominal point, we repeated the analysis at five further operating points obtained by multiplying each kinetic parameter by an independent factor in $[0.8, 1.25]$ and each order by a factor in $[0.92, 1.05]$ (capped at 0.999). The number of resolved directions ranged over $[7, 9]$, the number of practically unidentifiable parameters over $[8, 12]$ of 18, and the number of unidentifiable fractional orders over $[1, 2]$ of 4. The parameters classified as unidentifiable at every operating point were p_2, p_3, p_4, ω, σ, h_Y, Y_b, α_X. The qualitative verdict—that the insulin-action and glucagon blocks, including the order α_X of the unobserved insulin action, are not resolved by glucose–insulin sampling—is therefore stable within this range; individual borderline classifications (such as h or α_Y) are not.

5.3. **Profile likelihood.** The Fisher matrix is a local object, and its classification can be checked against the profile likelihood [33]. Using noise-free synthetic glucose and insulin data at the sampling times above, so that χ^2 vanishes at the nominal parameters, we fixed one parameter at $0.5, 0.7, 1.4$ and 2 times its nominal value and re-optimised

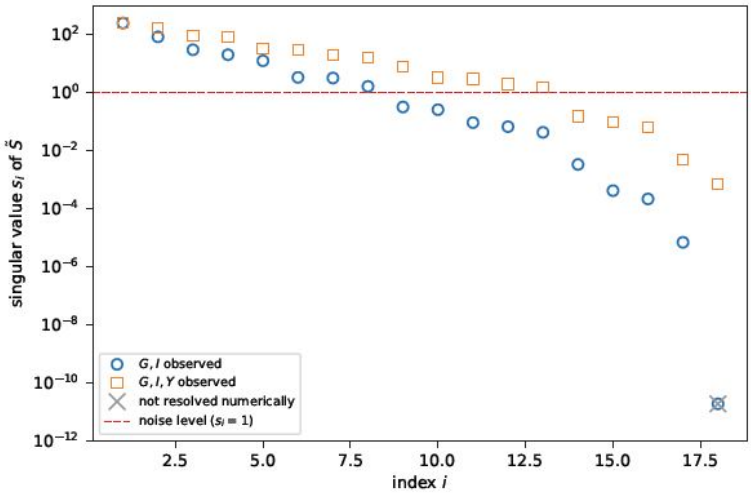

(A) Spectrum of the whitened sensitivity matrix.

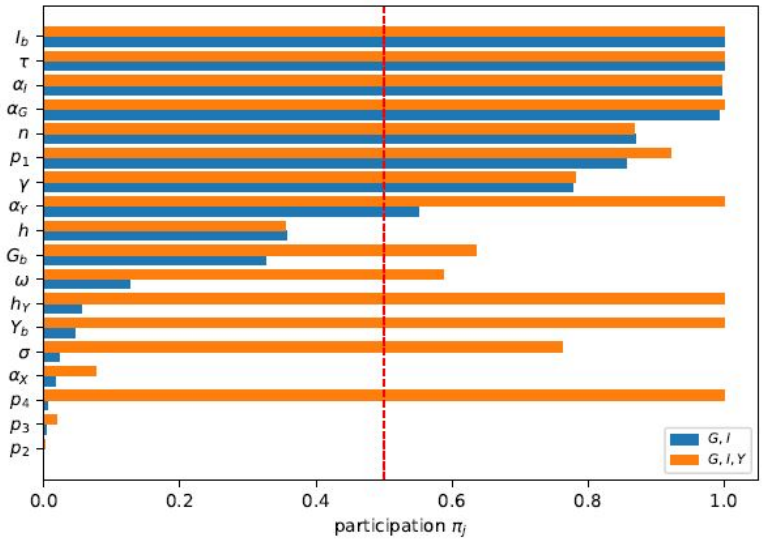

(B) Per-parameter participation.

FIGURE 2. (A) Singular values s_i of the whitened sensitivity matrix for glucose–insulin and glucose–insulin–glucagon sampling; dashed line: noise level $s_i = 1$; grey crosses: singular values that change by more than 1% when the computation is repeated at a higher resolution and are therefore not resolved numerically. (B) Participation π_j of each parameter in the resolved subspace; dashed line: $\pi_j = 1/2$.

the remaining seventeen (in logarithmic coordinates, within a factor of four of their nominal values and with the orders bounded by one) by a trust-region least-squares method. For noise-free data the profile value approximates the expected increase of χ^2 under the assumed noise, so a profile that stays below the pointwise 95% threshold $\Delta\chi^2 = 3.84$ indicates practical non-identifiability over the explored range. Because the optimiser is stopped after a finite number of function evaluations, the reported values are upper bounds on the profile. The forward model in this computation

is the ungraded method of steps with $M = 8$ (forward error below 10^{-4}), used both to generate the data and to fit them.

TABLE 5. Profile likelihood χ^2_{PL} (upper bounds, see text) for noise-free glucose–insulin data, with the profiled parameter fixed at the stated multiple of its nominal value. The pointwise 95% threshold is 3.84. *Optimiser stopped at the evaluation limit (the value is an upper bound). †For the order $\alpha_X \le 1$ the upward profile is evaluated at the bound $\alpha_X = 1$ (a factor 1/0.95).

Parameter	×0.5	×0.7	×1.4	×2	Classification (Table 4)
τ	10.85	5.18	4.23^{*}	15.45^{*}	identifiable
σ	$5 \times 10^{-4*}$	5×10^{-7}	$8 \times 10^{-7*}$	$8 \times 10^{-7*}$	structurally unidentifiable (symmetry)
p_2	4×10^{-8}	3×10^{-8}	$7 \times 10^{-11*}$	$1 \times 10^{-9*}$	practically unidentifiable
α_X	1×10^{-5}	7×10^{-7}	$1 \times 10^{-9\dagger}$	—	practically unidentifiable

Table 5 reports the results for the delay τ (identifiable), the α-cell responsivity σ (member of the structural symmetry), the insulin-action decay p_2 and the insulin-action order α_X. For τ, where the optimiser converged (factors 0.5 and 0.7), the profile is 10.8 and 5.2, above the threshold, so that a delay shortened by 30% cannot be absorbed by the other parameters. For the factors 1.4 and 2 the optimiser reached its evaluation limit at 4.2 and 15.4; these values are upper bounds, and the one at 1.4 lies only marginally above the threshold. The profile is therefore consistent with the local classification of τ as identifiable, with a pointwise 95% interval of the order of ±30–40% under the assumed design. The profile of σ remains at the level of the optimiser tolerance over the whole range (at most 5×10^{-4}, compared with the threshold 3.84), as predicted by the symmetry $(Y_b, \omega, \sigma) \mapsto (\lambda Y_b, \omega/\lambda, \lambda\sigma)$. The profiles of p_2 and α_X also stay far below the threshold, confirming their practical non-identifiability over a two-fold range. These four profiles agree with the local classification; a full profile study of all eighteen parameters, and under noisy data, is left for future work.

5.4. **An additional glucagon assay.** Adding glucagon measurements (same sampling times, $\sigma_Y = 1.4\,\mathrm{pg\,mL^{-1}}$) raises the number of resolved directions from $k = 8$ to $k = 13$. The parameters that change from unidentifiable to identifiable are p_4, ω, σ, h_Y, G_b, Y_b; in particular the structural symmetry is broken, since Y itself is now observed, and the glucagon order α_Y becomes clearly identifiable (participation from 0.55 to 1.00). The insulin-action parameters p_2, p_3, α_X remain unidentifiable (α_X: 0.08), because the remote state X is still unobserved, and so does the secretion threshold h, whose trade-off with γ and n is unaffected by glucagon data. Within this design, therefore, observing a compartment is what makes its parameters and its memory order recoverable; a glucagon assay does not compensate for the unobserved insulin action.

TABLE 6. Effect of the forward solver on the identifiability analysis (G, I observed). Forward error: maximum relative error of the observed states at the sampling times against the reference. k: number of singular values above one. Angle: largest principal angle between the resolved subspace and that of the reference computation (collocation, $M = 12$, $J = 4$, $k = 8$). $\Delta \log_{10} s$: largest change of a singular value above 10^{-3}. Sensitivity change: $\max|S - S_{\mathrm{ref}}| / \max|S_{\mathrm{ref}}|$.

Forward solver	Fwd. error	k	Angle (°)	$\Delta \log_{10} s$	Sens. change	Changed class.
spectral M=8, no grading	6.7×10^{-5}	8	0.32	0.04	1.1×10^{-2}	none
PECE h=0.005, interpolated delay	1.8×10^{-4}	8	0.07	0.03	6.5×10^{-3}	none
PECE h=0.01, interpolated delay	3.7×10^{-4}	8	0.17	0.19	3.9×10^{-2}	none
PECE h=0.05, interpolated delay	1.8×10^{-3}	8	0.60	0.21	2.2×10^{-1}	none
PECE h=0.1, interpolated delay	3.7×10^{-3}	8	1.06	0.23	5.5×10^{-1}	none
PECE h=0.01, delay rounded to grid	3.7×10^{-4}	8	0.39	0.14	6.5×10^{-2}	none
PECE h=0.1, delay rounded to grid	3.7×10^{-3}	7	—	1.10	1.0×10^{-1}	τ

Uncorrected Proof

5.5. **Sensitivity of the verdict to the forward solver.** A change in the sign of the smallest computed Fisher eigenvalue (of order 10^{-16}) between a coarse and a fine forward solution must not be interpreted as evidence that solver error corrupts the Fisher information: $F = \tilde{S}^\top \tilde{S}$ is positive semidefinite for any Jacobian, and eigenvalues of this magnitude are at the level of rounding in the eigendecomposition. We therefore use the following test, in which the complete analysis is repeated with forward solvers of widely different accuracy and the change of the resolved subspace is measured (Table 6).

When the delayed term is represented continuously, the verdict is insensitive to the forward accuracy over the range tested. Forward errors between 6.7×10^{-5} and 3.7×10^{-3} change individual sensitivities by up to 55% and singular values by up to 0.23 decades, but leave k and the classification unchanged, and the resolved subspace rotates by at most 1.1°. The accuracy of the solver thus affects the quantitative singular values but not, at this operating point, the qualitative conclusion. A material change arises from a different source: when the delay is rounded to the time grid, as is common in fixed-step implementations, $\partial/\partial\tau$ becomes a difference quotient of a piecewise-constant function of τ. With $h = 0.1$ the perturbation of τ does not move the rounded delay at all, the sensitivity to τ vanishes, k drops from 8 to 7, and τ is misclassified as unidentifiable; with $h = 0.01$ the rounded delay jumps by one grid step and the sensitivity to τ is quantised rather than differentiated. The requirement for a trustworthy verdict is therefore not a particular order of accuracy but a forward solver in which the parameters, including the delay, enter differentiably; the collocation scheme with moving interfaces satisfies this by construction.

6. Discussion

The question posed and the answer obtained. The recent fractional glucose–insulin literature has moved toward richer models—component-wise memory orders, discrete delays and, most recently, an explicit call for hormonal (glucagon) regulation [34]—while treating parameter recoverability either informally or as a corollary of well-posedness [5, 8]. Our analysis tests whether the enrichment is supported by the data ordinarily used to fit it. For the synthetic IVGTT design considered here (fourteen samples of glucose and insulin over thirty minutes, with the stated noise levels) the answer is largely negative: ten of the eighteen parameters of the enriched glucose–insulin–glucagon model, including the memory order α_X of the insulin-action compartment, are practically unidentifiable, and one combination of glucagon parameters is structurally unidentifiable. These statements refer to the assumed design and operating point; they indicate, rather than establish, what would happen with clinical data, for which the sampling schedule, the duration of the test and the noise differ.

Interpretation. The structure of the result is more informative than the count. The unidentifiable parameters are concentrated in the latent compartments: the insulin-action block (p_2, p_3, α_X) and the glucagon block (p_4, ω, σ, h_Y, Y_b). The memory order of a compartment was resolved in our computations when that compartment, or a compartment it drives directly, was observed: α_G and α_I were well determined, α_Y was marginal from glucose–insulin data and well determined once glucagon was measured, while α_X remained unresolved in every setting examined. This suggests a simple design heuristic—the fractional order of a state is best estimated from measurements of that state—which is consistent with, but not proven by, the present computations. It also qualifies the appeal of component-wise fractional orders: they add descriptive flexibility, but on the data considered here the orders of the hidden compartments are the parameters the data resolve least well. Remark 2.2 identifies one mechanism: through the factor $t_c^{1-\alpha}$, an order acts partly as a time-scale parameter and can trade off against the rate constants of its own equation.

Structural versus practical non-identifiability. The two notions should not be confused [33]. The scaling symmetry $(Y_b, \omega, \sigma) \mapsto (\lambda Y_b, \omega/\lambda, \lambda\sigma)$ is structural: glucose–insulin data, however dense or precise, cannot determine these three parameters separately, and the loss is removed only by changing the observation function (measuring Y) or by fixing one of them. All other losses reported here are practical: they depend on the fourteen-sample, thirty-minute design and on the assumed noise, and a longer or denser protocol, or lower noise, could in principle reduce them. In particular, after the bolus the glucagon secretion term is switched off until the delayed glucose falls below h_Y, which at the nominal point happens only at $t \approx 27$ min, in the last minutes of the window; a longer test that captures the glucose nadir would carry more information about the glucagon block.

Uncorrected Proof

Relation to prior identifiability work. That the classical minimal model can be numerically non-identifiable has been known since Pillonetto et al. [32], and practical identifiability limits have been documented for insulin kinetics [12], bihormonal control models [26], and ultradian oscillators [25]. Our contribution is to extend this scrutiny to the fractional, delayed, glucagon-coupled setting, to treat the fractional orders themselves as estimated parameters, and to document how the verdict depends on the forward computation. On the last point the conclusion is specific: over the range tested, the verdict was robust to forward accuracy as long as the delay entered the computation differentiably, whereas rounding the delay to a time grid changed the verdict for τ.

Limitations. Four limitations bound the claims. First, the parameter values are illustrative, not fitted to a specific cohort; the qualitative structure is stable across the operating points examined, but the exact per-parameter figures shift with the operating point, and borderline classifications (for example h and α_Y) are not robust. Second, the Fisher-information analysis is local; it was corroborated by profile likelihoods for four representative parameters, but a full profile study and an analysis under noisy data remain for future work. Third, the design is a single thirty-minute IVGTT; the conclusions should not be extrapolated to longer tests or to other protocols without repeating the analysis. Fourth, the classification thresholds ($s_i = 1$, $\pi_j = 1/2$) are conventions; parameters near them should be regarded as marginal.

7. Conclusions and recommendations

We assembled the four-state, delayed, fractional-order glucose–insulin–glucagon minimal model toward which the recent literature has been converging, wrote it in a dimensionally consistent form, solved it with a domain-decomposed hybrid Chebyshev–Legendre operational-matrix collocation scheme, and used the verified solver to ask whether the model's parameters are identifiable from standard intravenous glucose tolerance data. The main findings are the following.

(1) *Enrichment adds parameters that the standard design does not resolve.* From glucose and insulin sampling, ten of eighteen parameters, including the order α_X of the insulin-action compartment, are practically unidentifiable under the assumed design, and only eight singular directions of the whitened sensitivity matrix exceed the noise level.
(2) *The losses are concentrated in the unobserved compartments,* and the combination (Y_b, ω, σ) is structurally unidentifiable from glucose and insulin because of an exact scaling symmetry.
(3) *Extra measurements help selectively.* A glucagon assay restores the glucagon block, breaks the structural symmetry and makes the glucagon order identifiable, but it does not resolve the insulin-action parameters.
(4) *Numerical treatment of the breakpoints determines the solver accuracy.* Interfaces at the delay breakpoints and threshold-switching instants, geometric grading after the breakpoints at which the forcing jumps, and an exact treatment of the weakly singular memory integral at interface nodes are all required; together they reduce the error at $M = 16$ from 1.3×10^{-4} to 7×10^{-12}. The identifiability verdict at the nominal point was robust to forward accuracy, but not to rounding the delay to a time grid.

Two practical recommendations follow. Modellers should either fix the memory orders of unobserved compartments rather than estimate them, or extend the measurement protocol to the corresponding state; and identifiability verdicts for such models should be reported together with the forward solver used, its accuracy, and the way in which the delay enters the sensitivity computation. More broadly, the value of a richer physiological model is bounded not only by its fidelity but by the information content of the data used to identify it.

Future work will extend the profile-likelihood analysis to all parameters and to noisy data, examine longer and denser sampling designs, and calibrate the model against cohort IVGTT data to establish the clinical scope of the non-identifiability reported here.

Uncorrected Proof

Statements and declarations

Competing interests. The authors declare no competing interests.
Funding. No external funding was received for this work.
Data and code availability. All numerical results are reproducible with the script accompanying this submission

(`gig_pipeline.py`); no external data set is used, and the model parameters are listed in Table 1.

Use of AI tools. An AI assistant (Anthropic Claude) was used for literature triage, code prototyping, and language editing. All mathematical derivations, numerical computations, and conclusions were checked and validated by the authors, who take full responsibility for the content.

References

[1] M. Abbaszadeh, A. Ghoreyshi, and M. Dehghan, *A finite block method framework for nonlinear fractional integro-differential equations*, Math. Methods Appl. Sci., *49*(4) (2026), 2170–2188.

[2] K. I. A. Ahmed, S. M. Mirgani, A. Seadawy, and S. Saber, *A comprehensive investigation of fractional glucose–insulin dynamics: existence, stability, and numerical comparisons using residual power series and generalized Runge–Kutta methods*, J. Taibah Univ. Sci., *19*(1) (2025), 2460280.

[3] A. Alalyani, *Numerical solution of the fractional-order mathematical model of β-cells kinetics and glucose–insulin system using a predictor–corrector method*, Math. Models Comput. Simul., *14*(1) (2022), 159–171.

[4] M. Alhazmi, S. M. Mirgani, A. F. Aljohani, and S. Saber, *Numerical simulation of a fractional glucose–insulin model via successive approximation and ABM schemes*, AIMS Math., *10*(10) (2025), 22817–22849.

[5] M. Alhazmi, S. M. Mirgani, and S. Saber, *Hybrid Euler–Lagrange approach for fractional-order modeling of glucose–insulin dynamics*, Axioms, *14*(11) (2025), 800.

[6] M. H. Alshehri, F. Z. Duraihem, A. Alalyani, and S. Saber, *A Caputo (discretization) fractional-order model of glucose–insulin interaction: numerical solution and comparisons with experimental data*, J. Taibah Univ. Sci., *15*(1) (2021), 26–36.

[7] W. Banzi, I. Kambutse, V. Dusabejambo, E. Rutaganda, F. Minani, J. Niyobuhungiro, L. Mpinganzima, and J. M. Ntaganda, *Mathematical modelling of glucose–insulin system and test of abnormalities of type 2 diabetic patients*, Int. J. Math. Math. Sci., *2021* (2021), 6660177.

[8] M. Batool, M. Farman, A. S. Ghaffari, K. S. Nisar, and S. R. Munjam, *Analysis and dynamical structure of glucose insulin glucagon system with Mittag–Leffler kernel for type I diabetes mellitus*, Sci. Rep., *14*(1) (2024), 8058.

[9] R. N. Bergman, Y. Z. Ider, C. R. Bowden, and C. Cobelli, *Quantitative estimation of insulin sensitivity*, Am. J. Physiol., *236*(6) (1979), E667–E677.

[10] R. N. Bergman, L. S. Phillips, and C. Cobelli, *Physiologic evaluation of factors controlling glucose tolerance in man: measurement of insulin sensitivity and beta-cell glucose sensitivity from the response to intravenous glucose*, J. Clin. Invest., *68*(6) (1981), 1456–1467.

[11] K. Diethelm, N. J. Ford, and A. D. Freed, *A predictor–corrector approach for the numerical solution of fractional differential equations*, Nonlinear Dyn., *29*(1–4) (2002), 3–22.

[12] P. D. Docherty, J. G. Chase, T. F. Lotz, and T. Desaive, *A graphical method for practical and informative identifiability analyses of physiological models: a case study of insulin kinetics and sensitivity*, Biomed. Eng. Online, *10* (2011), 39.

[13] R. S. Dubey, D. Baleanu, M. N. Mishra, and P. Goswami, *Solution of modified Bergman minimal blood glucose–insulin model using Caputo–Fabrizio fractional derivative*, Comput. Model. Eng. Sci., *128*(3) (2021), 1247–1263.

[14] B. Erdős, S. D. O'Donovan, M. E. Adriaens, A. Gijbels, I. Trouwborst, K. M. Jardon, G. H. Goossens, L. A. Afman, E. E. Blaak, N. A. W. van Riel, and I. C. W. Arts, *Leveraging continuous glucose monitoring for personalized modeling of insulin-regulated glucose metabolism*, Sci. Rep., *14*(1) (2024), 8037.

[15] A. Ghoreyshi, M. Abbaszadeh, and M. Dehghan, *Hybrid L-type time discretization and spectral–finite block methods for nonlinear fractional PDEs with neutral delay*, Commun. Nonlinear Sci. Numer. Simul., *161* (2026), 110004.

[16] A. Ghoreyshi, M. Abbaszadeh, and M. Dehghan, *Numerical methods for the time-fractional diffusion equation: a review*, AUT J. Math. Comput., *7*(2) (2026), 213–269.

[17] A. Ghoreyshi, M. Abbaszadeh, M. A. Zaky, and M. Dehghan, *An accurate and robust numerical method for solving distributed-order space–time fractional PDEs*, Z. Angew. Math. Phys., *76*(6) (2025), 242.

Uncorrected Proof

[18] A. Ghoreyshi, M. Abbaszadeh, M. A. Zaky, and M. Dehghan, *Finite block method for nonlinear time-fractional partial integro-differential equations: stability, convergence, and numerical analysis*, Appl. Numer. Math., *214* (2025), 82–103.
[19] A. Ghoreyshi, M. Abbaszadeh, M. A. Zaky, and M. Dehghan, *Two high-order numerical schemes based on the Lagrange polynomials for solving a distributed-order time-fractional partial integro-differential equation on non-rectangular domains*, J. Appl. Math. Comput., *71*(5) (2025), 7271–7311.
[20] A. Ghoreyshi, M. A. Zaky, M. Abbaszadeh, and M. Dehghan, *An efficient numerical scheme for time-fractional partial integro-differential equations with time delay on rectangular and non-rectangular domains*, Comput. Appl. Math., *45*(10) (2026), 417.
[21] R. N. Gutenkunst, J. J. Waterfall, F. P. Casey, K. S. Brown, C. R. Myers, and J. P. Sethna, *Universally sloppy parameter sensitivities in systems biology models*, PLoS Comput. Biol., *3*(10) (2007), e189.
[22] M. W. Khan, M. Abid, and A. Q. Khan, *Fractional order Bergman's minimal model—a better representation of blood glucose–insulin system*, in: 2019 International Conference on Applied and Engineering Mathematics (ICAEM), IEEE, 2019, 68–73.
[23] S. R. Khirsariya, S. B. Rao, and G. S. Hathiwala, *Investigation of fractional diabetes model involving glucose–insulin alliance scheme*, Int. J. Dyn. Control, *12*(1) (2024), 1–14.
[24] K. Kumnungkit, C. Likasiri, R. Pongvuthithum, and F. Tantakitti, *Universal minimal model for glucose–insulin relationship with the influence of food dynamic*, Comput. Math. Methods Med., *2022* (2022), 8990767.
[25] M. E. Levine, G. Hripcsak, L. Mamykina, A. Stuart, and D. J. Albers, *Offline and online data assimilation for real-time blood glucose forecasting in type 2 diabetes*, arXiv preprint arXiv:1709.00163, 2017.
[26] C. Lopez-Zazueta, Ø. Stavdahl, and A. L. Fougner, *Low-order nonlinear animal model of glucose dynamics for a bihormonal intraperitoneal artificial pancreas*, IEEE Trans. Biomed. Eng., *69*(3) (2022), 1273–1280.
[27] S. Masroor, M. G. J. van Dongen, R. Alvarez-Jimenez, K. Burggraaf, L. A. Peletier, and M. A. Peletier, *Mathematical modeling of the glucagon challenge test*, J. Pharmacokinet. Pharmacodyn., *46*(6) (2019), 553–564.
[28] M. Morettini, L. Burattini, C. Göbl, G. Pacini, B. Ahrén, and A. Tura, *Mathematical model of glucagon kinetics for the assessment of insulin-mediated glucagon inhibition during an oral glucose tolerance test*, Front. Endocrinol., *12* (2021), 611147.
[29] Z. Öztürk, H. Bilgil, and S. Sorgun, *A new application of fractional glucose–insulin model and numerical solutions*, Sigma J. Eng. Nat. Sci., *42*(2) (2024), 407–413.
[30] G. Pacini and R. N. Bergman, *MINMOD: a computer program to calculate insulin sensitivity and pancreatic responsivity from the frequently sampled intravenous glucose tolerance test*, Comput. Methods Programs Biomed., *23*(2) (1986), 113–122.
[31] P. Palumbo, S. Ditlevsen, A. Bertuzzi, and A. De Gaetano, *Mathematical modeling of the glucose–insulin system: a review*, Math. Biosci., *244*(2) (2013), 69–81.
[32] G. Pillonetto, G. Sparacino, and C. Cobelli, *Numerical non-identifiability regions of the minimal model of glucose kinetics: superiority of Bayesian estimation*, Math. Biosci., *184*(1) (2003), 53–67.
[33] A. Raue, C. Kreutz, T. Maiwald, J. Bachmann, M. Schilling, U. Klingmüller, and J. Timmer, *Structural and practical identifiability analysis of partially observed dynamical models by exploiting the profile likelihood*, Bioinformatics, *25*(15) (2009), 1923–1929.
[34] S. Saber, E. Solouma, R. A. Alharb, and A. Alalyani, *Chaos in fractional-order glucose–insulin models with variable derivatives: insights from the Laplace–Adomian decomposition method and generalized Euler techniques*, Fractal Fract., *9*(3) (2025), 149.
[35] J. T. Sorensen, *A physiologic model of glucose metabolism in man and its use to design and assess improved insulin therapies for diabetes*, Ph.D. thesis, Department of Chemical Engineering, Massachusetts Institute of Technology, 1985.

Uncorrected Proof